Anatomy of the $0\nu\beta\beta$ nuclear matrix elements

Fedor Šimkovic,[1,*] Amand Faessler,[1] Vadim Rodin,[1] Petr Vogel,[2] and Jonathan Engel[3]

[1]*Institute für Theoretische Physik der Universität Tübingen, D-72076 Tübingen, Germany*
[2]*Kellogg Radiation Laboratory and Physics Department, Caltech, Pasadena, California 91125, USA*
[3]*Department of Physics and Astronomy, University of North Carolina, Chapel Hill, North Carolina 27599-3255, USA*

We show that, within the quasiparticle random phase approximation (QRPA) and the renormalized QRPA (RQRPA) based on the Bonn-CD nucleon-nucleon interaction, the competition between the pairing and the neutron-proton particle-particle and particle-hole interactions causes contributions to the neutrinoless double-beta decay matrix element to nearly vanish at internucleon distances of more than 2 or 3 fermis. As a result, the matrix element is more sensitive to short-range/high-momentum physics than one naively expects. We analyze various ways of treating that physics and quantify the uncertainty it produces in the matrix elements, with three different treatments of short-range correlations.

I. INTRODUCTION

Neutrino oscillations are firmly established (see, e.g., [1–5]) and demonstrate that neutrinos have masses many orders of magnitude smaller than those of charged leptons. But since the masses are nonzero, neutrinoless double-beta ($0\nu\beta\beta$) decay experiments will likely tell us sooner or later whether neutrinos are Majorana or Dirac particles [6–10]. Moreover, the rate of the $0\nu\beta\beta$ decay, or limits on it, can tell us about the absolute neutrino-mass scale and to some extent about the neutrino mass hierarchy.[1] But to achieve these goals we need an accurate evaluation of the nuclear matrix elements that govern the decay.

In this paper, which builds on previous publications [13,14] (which we call I and II), we analyze some of the physics affecting the nuclear matrix element $M^{0\nu}$—the competition between pairing and neutron-proton particle-particle correlations, the nonintuitive dependence of the decay amplitude on internucleon distance, and the treatment of short-range correlations and other high-momentum phenomena—that have not been sufficiently discussed before. As in our earlier papers (and most attempts to evaluate $M^{0\nu}$) we use the quasiparticle random phase approximation (QRPA) and its generalization, the renormalized QRPA (RQRPA), with an interaction obtained from the G matrix associated with the realistic Bonn-CD nucleon-nucleon interaction. That interaction, slightly renormalized, is used both as the like particle pairing and as the neutron-proton force. Where appropriate, we compare the results to those of the complementary large-scale shell model (LSSM).

The paper is organized as follows. In the next section, after briefly summarizing the relevant formalism, we show

that the final value of $M^{0\nu}$ reflects two competing forces: the like particle pairing interaction that leads to the smearing of Fermi levels and the residual neutron-proton interaction that, through ground state correlations, admixes "broken-pair" (higher-seniority) states. A partial cancellation between these interactions increases the sensitivity to their strengths. The same tendencies are present in the LSSM, as a recent paper shows [15]. (During the processing of this manuscript, a new paper on the LSSM appeared [16], emphasizing the competition again.) In Sec. III we discuss the dependence of $M^{0\nu}$ on the distance between the two neutrons that are converted into two protons. We show that the competition mentioned above implies that only internucleon distances $r_{ij} \lesssim$ 2–3 fm contribute. That fact, not recognized before, explains the sensitivity of the decay rate to higher order terms in nucleon currents, nucleon form factors, and short-range nucleon-nucleon repulsion. We show that the surprising dependence on the internucleon distance occurs not only in the QRPA but also in an exactly solvable model [17] that contains many ingredients of real nuclear systems. Short-range correlations have recently inspired a lively discussion [19–21] and we devote Sec. IV to various ways of treating them. In Sec. V we present numerical results for nuclei of experimental interest, that include a comprehensive analysis, within the QRPA method and its generalization, of the total uncertainty of the $0\nu\beta\beta$ nuclear matrix elements, and compare with results of the LSSM. Section VI summarizes our findings. Finally, in Appendix A we present formulas for two ways of evaluating the matrix elements, one via the evaluation of unsymmetrized two-body matrix elements (the procedure usually used) and another one through the product of two one-body matrix elements. And in Appendix B we show how to calculate shell-model particle-hole decompositions so they can be compared with those calculated in the QRPA.

II. FORMALISM AND MULTIPOLE DECOMPOSITIONS

Throughout we assume that the $0\nu\beta\beta$ decay, if observed, is caused by the exchange of the Majorana neutrinos, the same particles observed to oscillate. The half-life of the decay is

---

*On leave of absence from Department of Nuclear Physics, Comenius University, Mlynská dolina F1, SK–84215 Bratislava, Slovakia.

[1]Reference [11] discusses the goals and future direction of the field. Reference [12] discusses issues particularly relevant for the program of $0\nu\beta\beta$ decay search.

then

$$\frac{1}{T_{1/2}} = G^{0\nu}(E_0, Z)|M^{0\nu}|^2|\langle m_{\beta\beta}\rangle|^2, \quad (1)$$

where $G^{0\nu}(E_0, Z)$ is a precisely calculable phase-space factor and $M^{0\nu}$ is the nuclear matrix element. The effective Majorana neutrino mass $\langle m_{\beta\beta}\rangle$ is related to the absolute mass scale and oscillation parameters through

$$\langle m_{\beta\beta}\rangle = \sum_i^N |U_{ei}|^2 e^{i\alpha_i} m_i, \quad (\text{all } m_i \geqslant 0), \quad (2)$$

where U_{ei} is the first row of the neutrino mixing matrix and the α_i are unknown Majorana phases. Any uncertainty in $M^{0\nu}$ makes the value of $\langle m_{\beta\beta}\rangle$ equally uncertain.

As stated above, we use the QRPA and RQRPA methods based on the G matrix derived from the realistic Bonn-CD nucleon-nucleon force, i.e., the many body Hamiltonian is

$$H = \sum_{i=1}^A \frac{p_i^2}{2m_p} + \frac{1}{2}\sum_{i,j=1}^A V_{\text{G-matrix}}(i, j). \quad (3)$$

We describe in detail in Sec. V below the input used to solve the corresponding well-known equations of motion.

In the QRPA (and RQRPA) $M^{0\nu}$ is written as a sum over the virtual intermediate states, labeled by their angular momentum and parity J^π and indices k_i and k_f (explanations of the notation are in Appendix A, and in Ref. II):

$$\begin{aligned}
M_K &= \sum_{J^\pi, k_i, k_f, \mathcal{J}} \sum_{pnp'n'} (-1)^{j_n+j_{p'}+J+\mathcal{J}} \sqrt{2\mathcal{J}+1} \begin{Bmatrix} j_p & j_n & J \\ j_{n'} & j_{p'} & \mathcal{J} \end{Bmatrix} \\
&\times \langle p(1), p'(2); \mathcal{J}\|\bar{f}(r_{12})O_K\bar{f}(r_{12})\|n(1), n'(2); \mathcal{J}\rangle \\
&\times \langle 0_f^+||[c_{p'}^+\tilde{c}_{n'}]_J||J^\pi k_f\rangle\langle J^\pi k_f|J^\pi k_i\rangle \\
&\times \langle J^\pi k_i||[c_p^+\tilde{c}_n]_J||0_i^+\rangle.
\end{aligned} \quad (4)$$

The operators O_K, $K =$ Fermi (F), Gamow-Teller (GT), and Tensor (T) contain neutrino potentials and spin and isospin operators, and RPA energies $E_{J^\pi}^{k_i,k_f}$. The neutrino potentials, in turn, are integrals over the exchanged momentum q,

$$\begin{aligned}
&H_K\left(r_{12}, E_{J^\pi}^k\right) \\
&= \frac{2}{\pi g_A^2} R \int_0^\infty f_K(qr_{12}) \frac{h_K(q^2)q\,dq}{q + E_{J^\pi}^k - (E_i + E_f)/2}. \quad (5)
\end{aligned}$$

The functions $f_{F,GT}(qr_{12}) = j_0(qr_{12})$ and $f_T(qr_{12}) = j_2(qr_{12})$ are spherical Bessel functions (the sign of j_2 was given incorrectly in Ref. [14]). The functions $h_K(q^2)$ are defined in Appendix A and in Ref.II. The potentials depend explicitly, though rather weakly, on the energies of the virtual intermediate states, $E_{J^\pi}^k$. The function $\bar{f}(r_{12})$ in Eq. (4) represents the effects of short-range correlations. These will be discussed in detail in Sec. IV.

Two separate multipole decompositions are built into Eq. (4). One, already mentioned, is in terms the J^π of the virtual states in the intermediate nucleus, the good quantum numbers of the QRPA and RQRPA. The other decomposition is based on the angular momenta and parities $\mathcal{J}^\pi$ of the pairs of neutrons that are transformed into protons with the same

$\mathcal{J}^\pi$ (we drop the superscript π from now on for convenience). This latter representation is particularly revealing. In Fig. 1 we illustrate it both in the LSSM and QRPA, with the same single particle-spaces in each. These two rather different approaches agree in a semiquantitative way, but the LSSM entries for $\mathcal{J} > 0$ are systematically smaller in absolute value.

Reference [15] makes the claim that QRPA results are too large because they omit configurations with seniority greater than 4, which are especially effective in canceling the pairing part of the matrix element. This statement is not correct. The QRPA does include configurations with higher seniority (4, 8, 12, etc.) and, as Fig. 1 shows, the broken pair contributions to the matrix elements are as large or larger than in the LSSM. (Some of the difference might be due to differences in single-particle energies and occupation numbers, which are not identical in the two calculations even though the single-particle
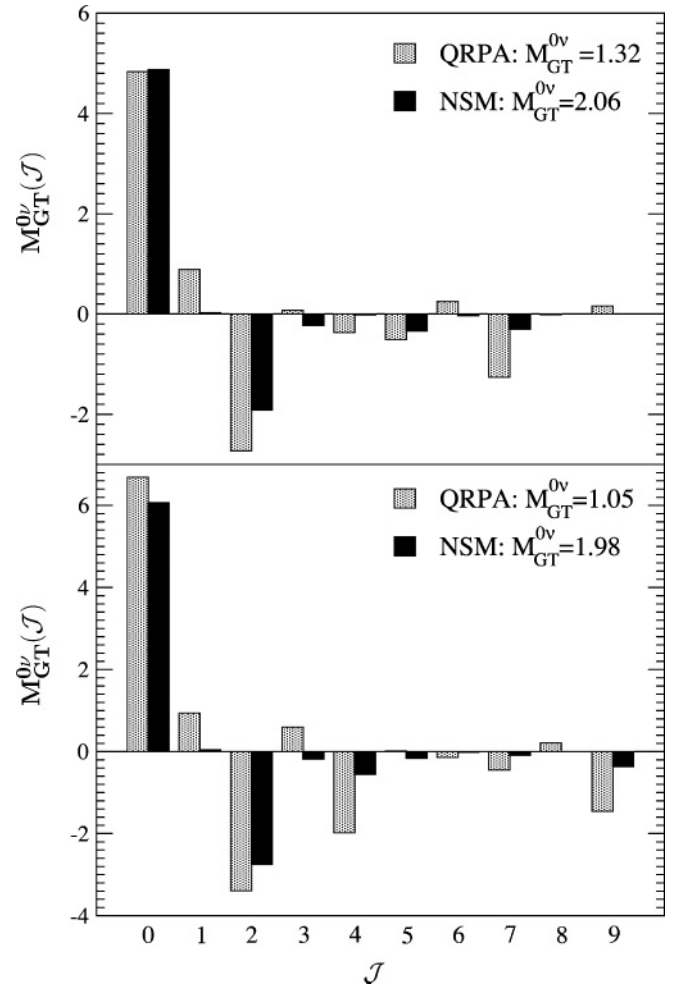

FIG. 1. Contributions of different angular momenta $\mathcal{J}$ associated with the two decaying neutrons to the Gamow-Teller part of $M^{0\nu}$ in ^{82}Se (upper panel) and ^{130}Te (lower panel). The results of LSSM (dark histogram) [23] and QRPA treatments (lighter histogram) are compared. Both calculations use the same single-particle spaces: $(f_{5/2}, p_{3/2}, p_{1/2}, g_{9/2})$ for ^{82}Se and $(g_{7/2}, d_{5/2}, d_{3/2}, s_{1/2}, h_{11/2})$ for ^{130}Te. In the QRPA calculation the particle-particle interaction was adjusted to reproduce the experimental $2\nu\beta\beta$-decay rate.
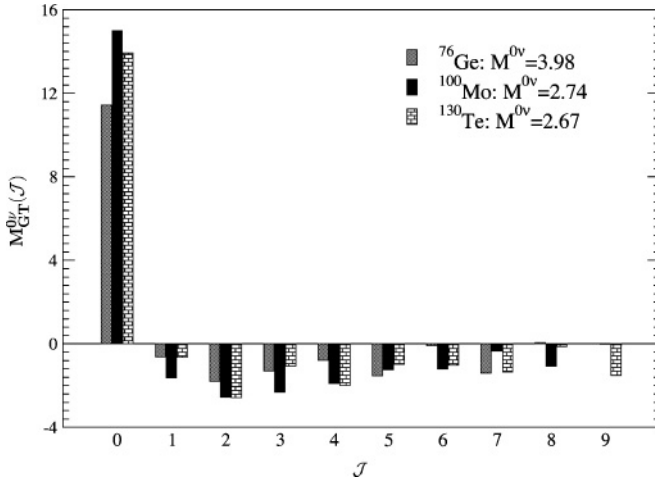
FIG. 2. Contributions of different angular momenta $\mathcal{J}$ associated with the two decaying neutrons to $M^{0\nu}$ in ^{76}Ge, ^{100}Mo and ^{130}Te. We use the QRPA, with the interaction strength g_{pp} adjusted so that the $2\nu\beta\beta$ lifetime is correctly reproduced. Short-range correlations are included the same way as in I and II.

wave functions are.) The reasons that the QRPA results presented in Sec. V are larger are a somewhat greater pairing contribution and contributions from negative parity multipoles that reinforce it. Most of the negative-parity contributions are absent from the shell model because of restrictions on the model space. These results suggest that the shell model is as likely to be missing important physics as is the QRPA. We return to this point in Sec. V.

In Fig. 2 we show the $\mathcal{J}$ decomposition for three nuclei in the QRPA, with single-particle spaces encompassing two major shells, a more natural span for this method. The cancellation between components with $\mathcal{J} = 0$ pairs and with $\mathcal{J} \neq 0$ pairs is always pronounced. The net $M^{0\nu}$ is considerably smaller than the pairing contribution and so depends rather sensitively on the pairing physics that determines the $\mathcal{J} = 0$ part, as well as on the strength of the proton-neutron force that determines the $\mathcal{J} \neq 0$ part.

From the structure of Eq. (4) and in particular from the form of the reduced matrix elements $\langle 0_f^+ || [c_{p'}^+ \tilde{c}_{n'}]_J || J^\pi k_f \rangle$ and $\langle J^\pi k_i || [c_p^+ \tilde{c}_n]_J || 0_i^+ \rangle$ it is obvious that only one of the two possible couplings between the neutron and proton operators in the two-body matrix element $\langle p(1), \ p'(2); \ \mathcal{J} || \bar{f}(r_{12}) O_K \bar{f}(r_{12}) || n(1), \ n'(2); \ \mathcal{J} \rangle$ is realized. This means that this two-body matrix element should not be antisymmetrized. In the LSSM one typically uses the closure approximation, which represents $M^{0\nu}$ as the ground-state-to-ground-state transition matrix element of a two-body operator. $M^{0\nu}$ can then be rewritten purely in terms of the antisymmetrized two-body matrix elements. After antisymmetrization, however, it is not possible to recover the decomposition into the multipoles J^π of the virtual intermediate states. In Appendix B we show how shell-model practitioners, by retaining unsymmetrized matrix elements, can decompose the matrix element into intermediate-state multipoles J^π for comparison with QRPA calculations. We cannot, however, make the comparison here without more shell-model data than has been published.
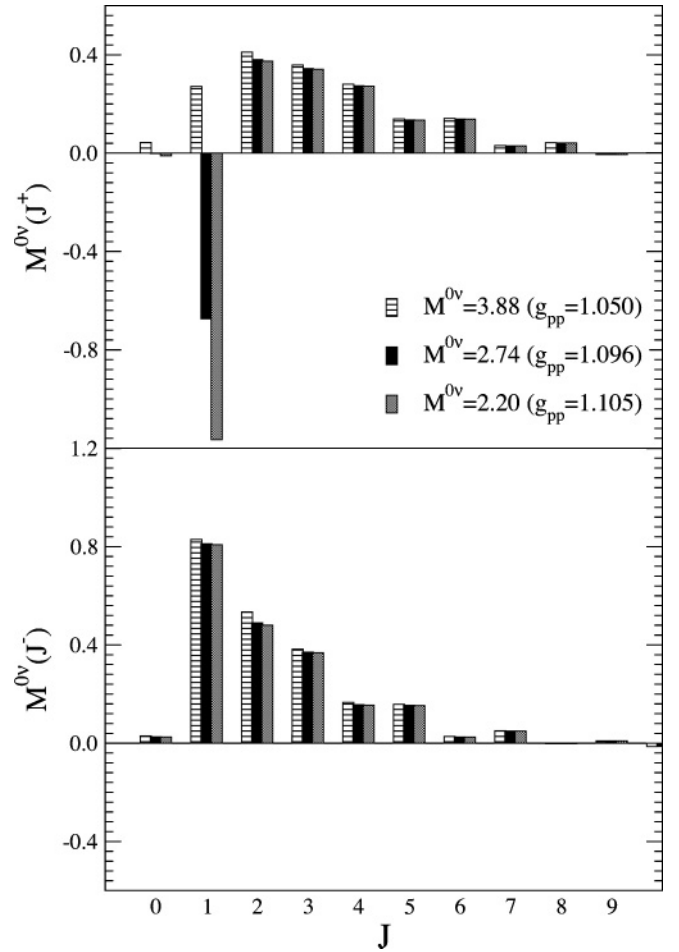

FIG. 3. The contributions of different intermediate-state angular momenta J to $M^{0\nu}$ in ^{100}Mo (positive parities in the upper panel and negative parities in the lower one). We show the results for several values of g_{pp}. The contribution of the 1^+ multipole changes rapidly with g_{pp}, while those of the other multipoles change slowly.

When using the QRPA or RQRPA to evaluate $M^{0\nu}$, one must fix several important parameters, the effects of which were discussed in detail in I and II. The strength g_{pp} by which we renormalize the Bonn-CD G matrix in the neutron-proton particle-particle channel is particularly important. We argued in I and II that g_{pp} should be chosen to reproduce the rate of two-neutrino $\beta\beta$ decay. This choice, among other things, essentially removes the dependence of $M^{0\nu}$ on the number of the single-particle states (or oscillator shells) in the calculations. The 2ν matrix element depends only on the 1^+ multipole. In Fig. 3 we show that it is essentially this multipole that is responsible for the rapid variation of $M^{0\nu}$ with g_{pp}. Fixing its contribution to a related observable (2ν decay) involving the same initial and final nuclear states appears to be an optimal procedure for determining g_{pp}.

III. DEPENDENCE ON THE DISTANCE BETWEEN THE NUCLEONS INVOLVED IN THE $0\nu\beta\beta$ TRANSITION.

The operators O_K in Eq. (4) depend on the distance r_{12} between the two neutrons that are transformed into

protons. The corresponding neutrino potentials are the Fourier transforms over the neutrino momentum q as shown in Eq. (5). Obviously, the range of r_{12} is restricted from above by $r_{12} \leqslant 2R_{\mathrm{nucl}}$. We show here, however, that in reality only much smaller values, $r_{12} \lesssim 2$–3 fm, or equivalently larger values of q, are relevant. Thus a good description of the physics involving distances $r_{12} \sim 1$ fm, or $q \sim 200$ MeV is important. That finding has not been recognized before, but perhaps it should be not so surprising that $q \sim p_{\mathrm{Fermi}}$ is the most relevant momentum transfer.

An example of the r_{12} dependence of $M^{0\nu}$ is shown in Fig. 4 for three nuclei. The quantity $C(r)$ is defined by evaluating $M^{0\nu}$ after multiplying $H^K(r', E^k_{J^\pi})$ by $r^2\delta(r - r')$, so that $C(r)$ is the contribution at r to $M^{0\nu}$, with $\int_0^\infty C(r)dr = M^{0\nu}$. As the lower panel of the figure demonstrates, the
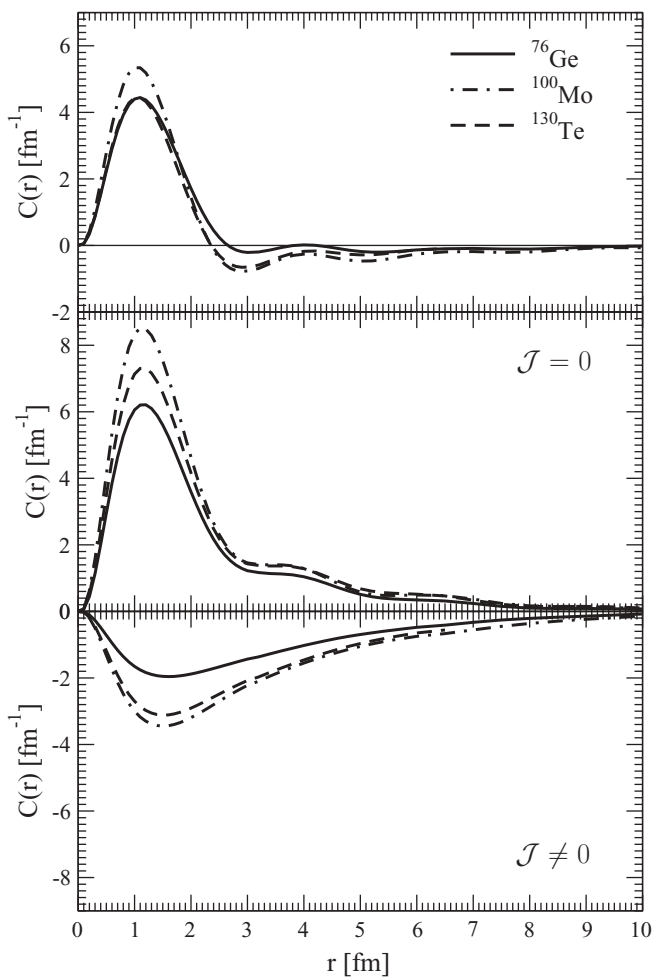

FIG. 5. The r_{12} dependence of $M^{0\nu}$ for ^{76}Ge, from calculations with different number of single-particle orbits. The dot-dashed curve was obtained with 21 s.p. subshells, the full curve with 12 subshells, the dashed curve with nine subshells, the dotted curve with six subshells, and the double dot-dashed curve with only four subshells.

cancellation between the $\mathcal{J} = 0$ and $\mathcal{J} \neq 0$ components is essentially complete for $r_{12} \gtrsim 2$–3 fm. Since the typical distance from a particular nucleon to its nearest neighbor is ~ 1.7 fm (because $R_{\mathrm{nucl}} = 1.2A^{1/3}$) the nucleons participating in the $0\nu\beta\beta$ decay are mostly nearest neighbors. Short-range nucleon-nucleon repulsion, the finite nucleon size, represented by nucleon form factors, and components of the weak currents that are typically suppressed by q/M_{nucleon} are therefore more important than one would naively expect.

Perhaps the most interesting thing about the figure is that the pairing and nonpairing parts of $C(r)$ taken individually (as in the two panels of the figure) extend to significantly larger r. The cancellation between them, that we discussed earlier, is particularly effective beyond 2 or 3 fm, leaving essentially nothing there. Figure 5 shows that the shape of $C(r)$, like the integrated matrix element, is essentially independent of the number of single-particle orbits included, as long as the truncation is not too severe (as it is with the dash-double-dot curve, for which important spin-orbit partners were omitted— only the four single particle states $p_{3/2}$, $p_{1/2}$, $f_{5/2}$, $g_{9/2}$ were included) and the coupling constant g_{pp} is chosen to reproduce the measured $2\nu\beta\beta$ lifetime. For other values of g_{pp} the cancellation between the $\mathcal{J} = 0$ and $\mathcal{J} \neq 0$ contributions at r larger than 2 or 3 fm is not as complete as in Fig. 4. We return to this point shortly.

We show the r_{12} dependence of the different parts of the $M^{0\nu}$ in Fig. 6. All individual contributions die out at r larger than 2 or 3 fm. The pseudoscalar-axial vector interference part has opposite sign from the other contributions, and essentially (and accidentally) cancels the contributions of the vector, weak magnetism and pure pseudoscalar pieces. The higher-order terms reduce the matrix element noticeably, and have to be included.

To gain some insight into the renormalization of the double-beta decay operator in the shell model, Ref. [17] employs a solvable model based on the algebra $SO(5) \times SO(5)$. The valence space contains two major shells ($fpg_{9/2}$ and $sdg_{7/2}$),

FIG. 4. The dependence on r_{12} of $M^{0\nu}$ for ^{76}Ge, ^{100}Mo, and ^{130}Te. The upper panel shows the full matrix element, and the lower panel shows separately 'pairing' ($\mathcal{J} = 0$ for the two decaying neutrons) and 'broken pair' ($\mathcal{J} \neq 0$) contributions. The integrated matrix element is 5.35 for ^{76}Ge, 4.46 for ^{100}Mo, and 4.09 for ^{130}Te. The g_{pp} values that reproduce the known $T_{1/2}^{2\nu}$ are 1.030, 1.096, and 0.994. The single-particle space for ^{76}Ge contains nine levels (oscillator shells $N = 3, 4$), and that for ^{100}Mo and ^{130}Te contains 13 levels (oscillator shells $N = 3, 4$ plus the f and h orbits from $N = 5$). Short-range correlation are not included, i.e., $\bar{f}(r_{12}) = 1$ in Eq. (4).
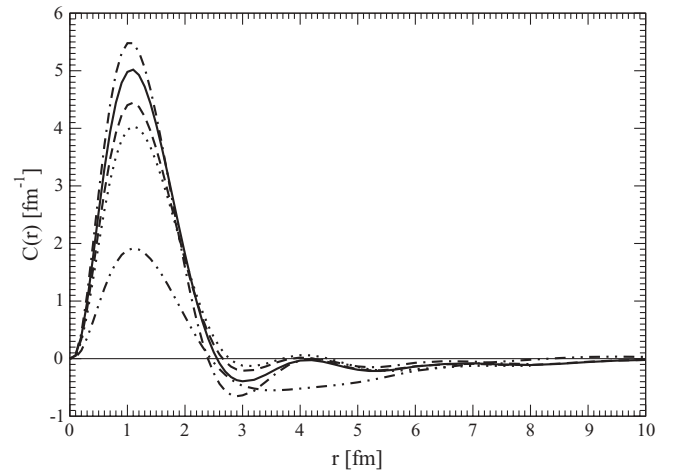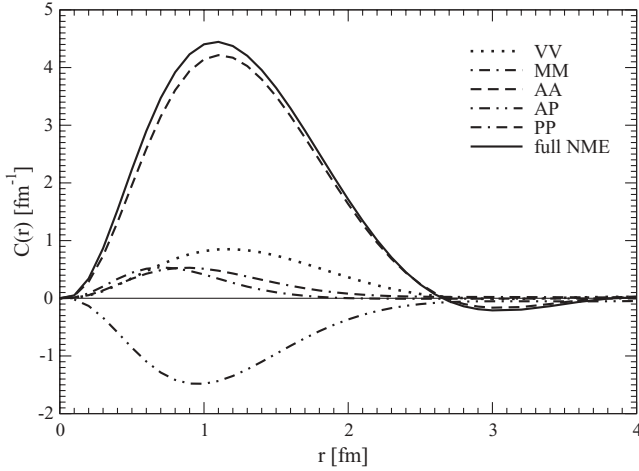
FIG. 6. The r_{12} dependence of the contributions of various pieces of $M^{0\nu}$ for ^{76}Ge are shown. Here AA stands for axial, VV for vector, AP for axial-pseudoscalar interference, PP for pseudoscalar, and MM for weak-magnetism. For definitions see Appendix A, or Ref. [22]. The model space contains nine subshells.

split by an energy ϵ, with degenerate levels within each shell. The single-particle wave functions are taken from a harmonic oscillator with $\hbar\omega$ =9.2 MeV. The Hamiltonian (for this schematic model only, not in the rest of the paper) is

$$H = \epsilon\hat{N}_2 - G\sum_{a,b=1}^{2}\left(S_{pp}^{\dagger a}S_{pp}^{b} + S_{nn}^{\dagger a}S_{nn}^{b} + g_{pp}S_{pn}^{\dagger a}S_{pn}^{b}\right.$$
$$\left. - g_{ph}\boldsymbol{T}_a\cdot\boldsymbol{T}_b\right), \tag{6}$$

where $a, b = 1, 2$ label the shells (lower and upper), ϵ is the energy difference between the shells, $\hat{N}_2$ is the number operator for the upper shell, $\boldsymbol{T}_a$ is total isospin operator for shell a, and

$$S_{pp}^{\dagger a} = \frac{1}{2}\sum_{\alpha\in a}\hat{j}_\alpha[\pi_\alpha^\dagger\pi_\alpha^\dagger]_0^0,$$
$$S_{nn}^{\dagger a} = \frac{1}{2}\sum_{\alpha\in a}\hat{j}_\alpha[\nu_\alpha^\dagger\nu_\alpha^\dagger]_0^0, \tag{7}$$
$$S_{pn}^{\dagger a} = \frac{1}{\sqrt{2}}\sum_{\alpha\in a}\hat{j}_\alpha[\pi_\alpha^\dagger\nu_\alpha^\dagger]_0^0.$$

Here $\pi_\alpha^\dagger$ ($\nu_\alpha^\dagger$) creates a proton (neutron) in level α with angular momentum j_α, $\hat{j} \equiv \sqrt{2j+1}$, and the square brackets indicate angular-momentum coupling. H contains only generators of $SO(5) \times SO(5)$, so its lowest lying eigenstates consist of configurations in which the nucleons are entirely bound in isovector S pairs of the type in Eq. (7).

This model has no active spin, so it is only suitable for calculating Fermi (neutrinoless) double-beta decay. To simulate the effect of g_{pp} on Gamow-Teller decay we change the Fermi matrix element by varying the strength of isovector neutron-proton pairing, in the same way that we change the Gamow-Teller matrix element in the realistic QRPA by varying the strength of isoscalar pairing. The advantage of this model is that we can solve it exactly rather than in the QRPA.
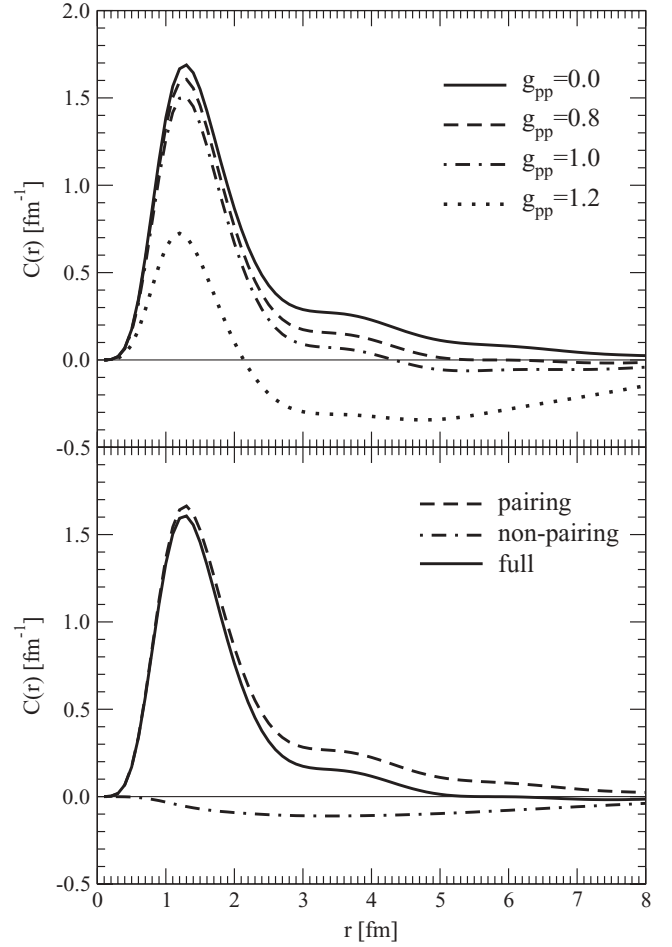

FIG. 7. The r_{12} dependence of $M^{0\nu}$ in the exactly solvable model for four values of g_{pp} (upper panel). The integrated matrix elements are 2.93 for $g_{pp} = 0$ and 1.69 for $g_{pp} = 1$. The lower panel shows separately the contributions of $\mathcal{J} = 0$ pairs and $\mathcal{J} \neq 0$ pairs for $g_{pp} = 0.8$.

We can use the model to test the $\boldsymbol{r}_{12}$-dependence of the double-beta decay matrix element in an exact solution. (Analytic expressions for the necessary matrix elements are in Ref. [17].) The upper panel of Fig. 7 shows the dependence for several values of g_{pp}, with $g_{ph} = 0$ and $\epsilon = 10G$. Just as in the realistic QRPA calculations, the contribution beyond $r = 3$ fm is very small for g_{pp} around 1; it is too small to distinguish from zero in the figure beyond 5 fm for $g_{pp} = 0.8$. However, for other values, as noted above, the large-r contributions can be substantial. The bottom panel divides the function into like-particle pairing and nonpairing parts for $g_{pp} = 0.8$. The two cancel to high precision at large r. The suppression at long ranges we observe in the QRPA, then, appears to be fairly general. It happens even in a very simple model, solved exactly. (As noted above, a new preprint [18] appeared during the processing of this manuscript. In it the r_{12} dependence of the $M^{0\nu}$, as well as the dependence of the separated pairing and broken-pair contributions, was evaluated in the LSSM. That analysis, inspired by our work, yielded curves that are strikingly similar to those in Fig. 4.)

IV. SHORT-RANGE CORRELATIONS AND OTHER HIGH-MOMENTUM PHENOMENA

Since only $r_{12} \lesssim 2$–3 fm, [equivalently $q > \hbar c/(2$–3 fm)], contributes to $M^{0\nu}$, some otherwise negligible effects become important. These effects are not commonly included, or included only in rough approximation, in nuclear-structure calculations. For example, the dipole approximation for nucleon form factors and the corresponding parameters M_V and M_A come from electron and neutrino charged-current-scattering from on-shell nucleons. Nuclear structure deals with bound nucleons and virtual neutrinos that are far off-shell. Similarly, the induced pseudoscalar current, with its strength obtained from the Goldberger-Treiman relation, has been tested in muon capture on simple systems. Here we are using this current for off-shell virtual neutrinos. Short range nucleon-nucleon repulsion has been considered carefully when calculating nuclear binding energies, but here we need its effect on a transition operator connecting two different nuclear ground states. All these effects will introduce some uncertainty because their treatment is not well tested. Nevertheless, it is important to understand their size at least roughly.

To show the importance of high momenta explicitly, we display in Fig. 8 the q dependence $C(q)$—defined in complete
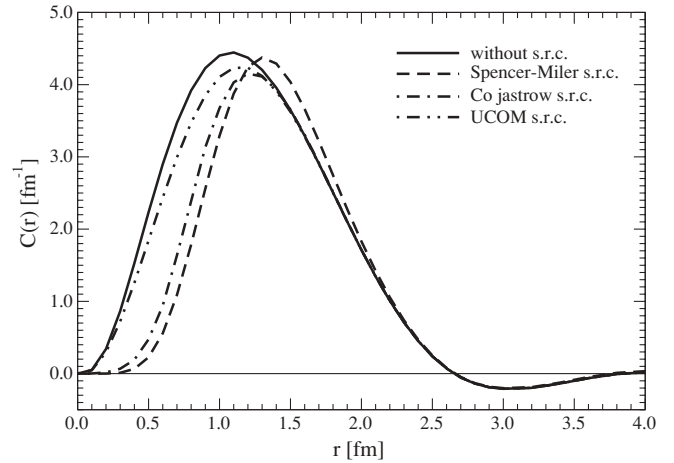
FIG. 9. The r_{12} dependence of $M^{0\nu}$ in ^{76}Ge evaluated in the model space that contains nine subshells. The four curves show the effects of different treatments of short-range correlations. The resulting $M^{0\nu}$ values are 5.32 when the effect of short range correlations is ignored, 5.01 when the UCOM transformation [24] is applied, 4.14 when the $\bar{f}(r_{12})$ from Fermi hypernetted-chain calculations [25] is used in Eq. (4), and 3.98 when the phenomenological Jastrow $\bar{f}(r_{12})$ is used [26].

analogy to $C(r)$—of $M^{0\nu}$ in ^{76}Ge, in a similar manner to which we exhibited the r_{12} dependence earlier. The cancellation between the $\mathcal{J} = 0$ and $\mathcal{J} \neq 0$ parts is particularly complete at lower values of q so that the resulting curve in the upper panel, although reduced in magnitude, is clearly shifted toward higher q.

The first high-momentum effect we examine is short-range correlations. Figure 9 displays the r_{12} dependence of $M^{0\nu}$ for several methods of handling short-range physics. For obvious reasons all methods reduce the magnitude of $M^{0\nu}$. The Unitary Correlation Operator Method (UCOM) [24] leads to the smallest reduction, less than 5%. The phenomenological Jastrow-like function $\bar{f}(r_{12})$ in Eq. (4) (from Ref. [26]) reduces $M^{0\nu}$ by about 20%. We also display the results of using a microscopically-derived Jastrow function [25]; its effect is similar to that of the phenomenological function. Since it is not clear which approach is best, we believe it prudent to treat the differences as a relatively modest uncertainty.

Nucleon form factors pose fewer problems because it turns out that once the short-range correlations effects are included, no matter how, the form factors are almost irrelevant as long as the cut-off masses $M_{A,V}$ are at least as large as the standard values ($M_A = 1.09$ GeV and $M_V = 0.85$ GeV). In Fig. 10 we show the dependence of $M^{0\nu}$ on the values of $M_{A,V}$ which for this purpose are set equal to each other, with three alternatives for treating short-range correlations. By 2 GeV the curves have essentially reached the infinite-mass limit. Since they are essentially flat past 1 GeV for both the UCOM and Jastrow-like prescriptions, including the form factors causes only minor changes in $M^{0\nu}$. Only if the correlations are ignored altogether do the form factors make a significant difference.

Finally, there is little doubt that the higher order weak currents, induced pseudoscalar and weak magnetism, should be included in the calculation. Even though the Goldberger-
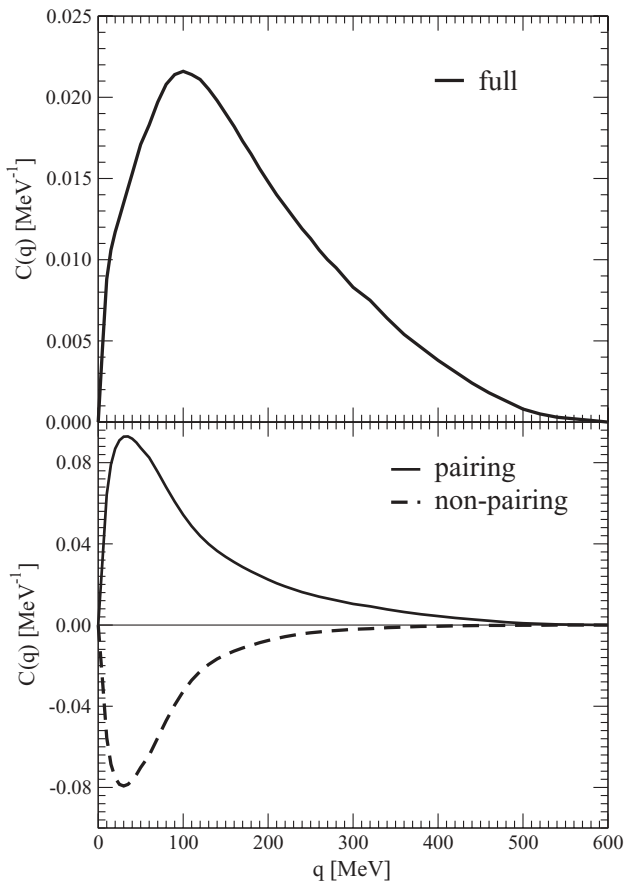

FIG. 8. The momentum-transfer dependence of $M^{0\nu}$ in ^{76}Ge. The upper panel is for the full matrix element; in the lower panel we separate the $\mathcal{J} = 0$ and $\mathcal{J} \neq 0$ parts. The scale is different in the two panels. The model space contains nine subshells.
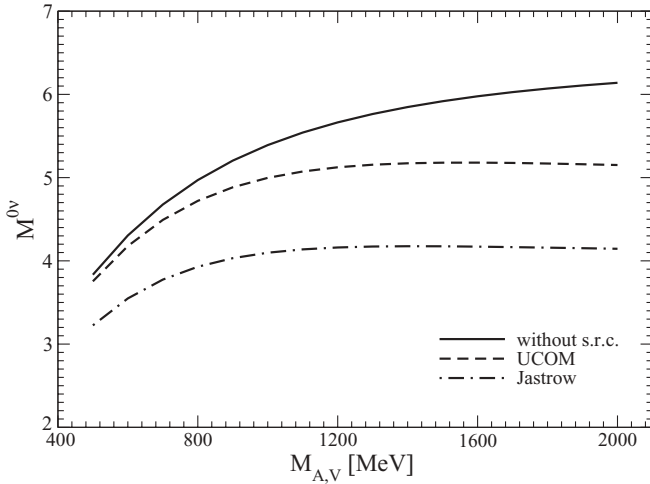
FIG. 10. The dependence of $M^{0\nu}$ in ^{76}Ge on the value of the dipole-form-factor cut-off parameters $M_{A,V}$. The upper curve was calculated without short range correlations, while the two lower curves were obtained with the UCOM and Jastrow methods. The two lower curves, unlike the upper one, are essentially flat for $M_{A,V}$ larger than the standard value of $\approx$1 GeV.

Treiman relation has not been tested in two-body operators, the relation is sufficiently well established that we do not associate a sizable uncertainty with its use.

V. NUMERICAL RESULTS

Figure 11 shows our calculated ranges for $M'^{0\nu}$, defined as $M'^{0\nu} = (g_A/1.25)^2 M^{0\nu}$ to allow us to display the effects of uncertainties in g_A. Such a definition allows us to use the same phase space factor $G^{0\nu}$ with $g_A = 1.25$ when calculating the 0νββ-decay rate.

We consider the effects of short-range correlations an uncertainty, since we do not know the best way of treating them. The error bars in Fig. 11 represent the difference between the highest and lowest of 24 calculations—in either
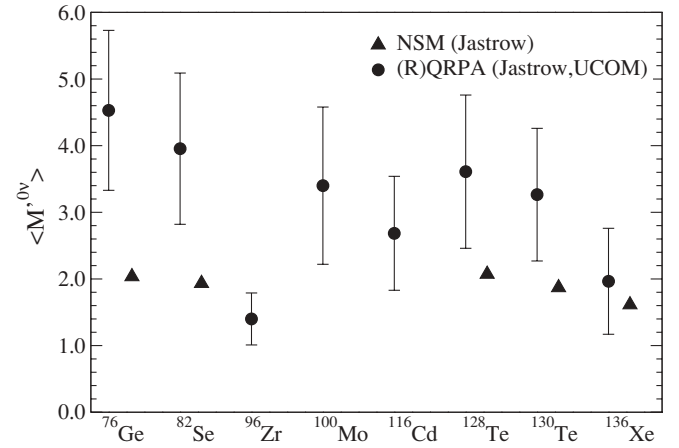

FIG. 11. Circles represent the mean value of the upper and lower limits of our calculated values of $M'^{0\nu}$; see text for description of error bars. For comparison the results of a recent large scale shell model evaluation of $M'^{0\nu}$ that used the Jastrow-type treatment of short range correlations are also shown as triangles.

the QRPA or RQRPA, each with three different sets of single-particle states (usually two, three, and four oscillator shells), two values for the in-medium g_A (1.0 and 1.25), and two treatments of short-range correlations (phenomeological Jastrow functions and the UCOM method)—and include the experimental uncertainty in the values of the 2ν lifetimes used to determine g_{pp}. Thus the error bars displayed in Fig. 11 represent our estimate of the full uncertainty in the 0νββ matrix elements within the QRPA and RQRPA methods. Though the results are in reasonable agreement with those presented in Refs. [20,21], the uncertainties are different.

Reference [16] presents new LSSM results for $M'^{0\nu}$, the values of which are shown also in Fig. 11. They are somewhat smaller than the QRPA values for ^{76}Ge and ^{82}Se and in a fair agreement for ^{116}Cd, ^{128}Te, ^{130}Te, and ^{136}Xe. Various nuclear-structure effects may be responsible for the

TABLE I. The calculated ranges of the nuclear matrix element $M'^{0\nu}$ evaluated within both the QRPA and RQRPA and with both standard ($g_A = 1.254$) and quenched ($g_A = 1.0$) axial-vector couplings. In each case we adjusted g_{pp} so that the rate of the 2νββ = decay is reproduced. Column 2 contains the ranges of $M'^{0\nu}$ with the phenomenological Jastrow-type treatment of short-range correlations (see I and II), while column 3 shows the UCOM-based results (see Ref. [24]). Columns 3 and 5 give the 0νββ-decay half-life ranges corresponding to the matrix-element ranges in columns 2 and 4, for $\langle m_{\beta\beta}\rangle = 50$ meV.

Nuclear transition	(R)QRPA (Jastrow s.r.c.)		(R)QRPA (UCOM s.r.c.)	
	$M'^{0\nu}$	$T_{1/2}^{0\nu}$ ($\langle m_{\beta\beta}\rangle = 50$ meV)	$M'^{0\nu}$	$T_{1/2}^{0\nu}$ ($\langle m_{\beta\beta}\rangle = 50$ meV)
^{76}Ge → ^{76}Se	(3.33, 4.68)	(6.01, 11.9) × 10²⁶	(3.92, 5.73)	(4.01, 8.57) × 10²⁶
^{82}Se → ^{82}Kr	(2.82, 4.17)	(1.71, 3.73) × 10²⁶	(3.35, 5.09)	(1.14, 2.64) × 10²⁶
^{96}Zr → ^{96}Mo	(1.01, 1.34)	(7.90, 13.9) × 10²⁶	(1.31, 1.79)	(4.43, 8.27) × 10²⁶
^{100}Mo → ^{100}Ru	(2.22, 3.53)	(1.46, 3.70) × 10²⁶	(2.77, 4.58)	(8.69, 23.8) × 10²⁵
^{116}Cd → ^{116}Sn	(1.83, 2.93)	(1.95, 5.01) × 10²⁶	(2.18, 3.54)	(1.34, 3.53) × 10²⁶
^{128}Te → ^{128}Xe	(2.46, 3.77)	(3.33, 7.81) × 10²⁷	(3.06, 4.76)	(2.09, 5.05) × 10²⁷
^{130}Te → ^{130}Xe	(2.27, 3.38)	(1.65, 3.66) × 10²⁶	(2.84, 4.26)	(1.04, 2.34) × 10²⁶
^{136}Xe → ^{136}Ba	(1.17, 2.22)	(3.59, 12.9) × 10²⁶	(1.49, 2.76)	(2.32, 7.96) × 10²⁶

discrepancies. More complicated configurations in LSSM that are absent in QRPA typically reduce $M^{0\nu}$ and could make most of the difference. On the other hand, in the QRPA includes more single particle states than in LSSM. That has the tendency to increase $M^{0\nu}$ and could also be responsible for the discrepancy. As we said earlier, the notion that the QRPA omits high-seniority states is not correct and should not be used to argue that the LSSM results are more accurate.

Given the interest in the subject, we show the range of predicted half-lives corresponding to our full range of $M'^{0\nu}$ in Table I (for $\langle m_{\beta\beta}\rangle = 50$ meV). As we argued above, this is a rather conservative range within the QRPA and its related frameworks. One should keep in mind, however, the discrepancy between the QRPA and LSSM results as well as systematic effects that might elude either or both calculations.

VI. CONCLUSIONS

The most important and novel result here is that the generic competition between $\mathcal{J} = 0$ (pairing) and $\mathcal{J} \neq 0$ (broken pair) multipoles leads to almost complete cancellation of the contribution to the matrix element from internucleon distances $r \gtrsim 2$–3 fm. That explains why the effects that depend on smaller values of r, or equivalently larger momentum transfers q, become important. This competition also means that the final matrix elements have enhanced sensitivity to the strengths of these interactions. Despite the uncertainties associated with the short range effects, we conclude that a proper fitting of the QRPA and/or RQRPA parameters leads to a relatively narrow range for $M'^{0\nu}$, with a smooth dependence (^{96}Zr being an exception) on atomic charge and mass.

We evaluate the values of the matrix elements for nuclei of experimental interest and display our best estimate of the corresponding spread. Part of that spread is associated with the difference in the size of the single particle space and whether QRPA or RQRPA is used, as discussed earlier in I and II. An interesting new conclusion is that short-range correlations, no matter how they are treated, essentially eliminate the effect of finite nucleon size on the matrix elements. But we still do not know the best way to treat the correlations, a fact that contributes about 20% to uncertainties presented above. The uncertainty in the effective value of g_A contributes about 30%, with the rest due to choice of method and model space, and the experimental uncertainty in 2ν lifetimes.

ACKNOWLEDGMENTS

APPENDIX A

Here we outline the derivation of $M^{0\nu}$, emphasizing induced (higher-order) currents. We assume light-neutrino exchange throughout, and the standard lepton×hadron weak charged-current Hamiltonian. The hadronic current, expressed in terms of nucleon fields Ψ, is

$$j^{\rho\dagger} = \overline{\Psi}\tau^+\left[g_V(q^2)\gamma^\rho + ig_M(q^2)\frac{\sigma^{\rho\nu}}{2m_p}q_\nu \right.$$
$$\left. - g_A(q^2)\gamma^\rho\gamma_5 - g_P(q^2)q^\rho\gamma_5\right]\Psi, \quad (A1)$$

where m_p is the nucleon mass and q^μ is the momentum transfer, i.e., the momentum of the virtual neutrino. Since in the $0\nu\beta\beta$ decay $\vec{q}^2 \gg q_0^2$ we take $q^2 \simeq -\vec{q}^2$. For the vector and axial vector form factors we adopt the usual dipole approximation $g_V(\vec{q}^2) = g_V/(1 + \vec{q}^2/M_V^2)^2$, $g_A(\vec{q}^2) = g_A/(1 + \vec{q}^2/M_A^2)^2$, with $g_V = 1$, $g_A = 1.254$, $M_V = 850$ MeV, and $M_A = 1086$ MeV. We use the usual form for weak magnetism, $g_M(\vec{q}^2) = (\mu_p - \mu_n)g_V(\vec{q}^2)$, and the Goldberger-Treiman relation, $g_P(\vec{q}^2) = 2m_p g_A(\vec{q}^2)/(\vec{q}^2 + m_\pi^2)$, for the induced pseudoscalar term.

To derive the expression for the matrix element we follow the procedure outlined in Ref. [27], arriving after a few steps at an expression for the $0_i^+ \to 0_f^+$ ground state to ground state transition:

$$M^{0\nu} = \frac{4\pi R}{g_A^2}\int\left(\frac{1}{(2\pi)^3}\int\frac{e^{-i\vec{q}\cdot(\vec{x}_1-\vec{x}_2)}}{|q|}\right)$$
$$\times \sum_m \frac{\langle 0_f^+|J_\alpha^\dagger(\vec{x}_1)|m\rangle\langle m|J^{\alpha\dagger}(\vec{x}_2)|0_i^+\rangle}{E_m - (E_i+E_f)/2 + |q|}d\vec{q}\,d\vec{x}_1 d\vec{x}_2.$$
$$(A2)$$

We have made the (accurate) approximation that all electrons are emitted in the $s_{1/2}$ state, with energies equal to half the available energy $(E_i - E_f)/2$. The normalization factor $4\pi R/g_A^2$, introduced for convenience, is compensated for by corresponding factors in the phase space integral.

Reducing the nucleon current to the nonrelativistic form yields (see Ref. [28]) in Eq. (A2):

$$J^{\rho\dagger}(\vec{x}) = \sum_{n=1}^A \tau_n^+\left[g^{\rho0}J^0(\vec{q}^2) + \sum_k g^{\rho k}J_n^k(\vec{q}^2)\right]\delta(\vec{x}-\vec{r}_n),$$
$$(A3)$$

where $J^0(\vec{q}^2) = g_V(q^2)$ and

$$\vec{J}_n(\vec{q}^2) = g_M(\vec{q}^2)i\frac{\vec{\sigma}_n\times\vec{q}}{2m_p} + g_A(\vec{q}^2)\vec{\sigma} - g_P(\vec{q}^2)\frac{\vec{q}\,\vec{\sigma}_n\cdot\vec{q}}{2m_p},$$
$$(A4)$$

$\vec{r}_n$ is the coordinate of the nth nucleon, $k = 1, 2, 3$, and $g^{\rho,\alpha}$ is the metric tensor.

The two current operators in $M^{0\nu}$ lead to an expression in terms of five parts [22]:

$$M^{0\nu} = M_{VV} + M_{MM} + M_{AA} + M_{AP} + M_{PP}, \quad (A5)$$

with the notation indicating which parts (axial, vector, etc.) of the nucleon current contribute. After integrating over $d\vec{x}_1, d\vec{x}_2$,

and $d\Omega_q$ in Eq. (A3) and writing one-body charge-changing operators in second quantization as

$$\hat{\mathcal{O}}_{JM} = \sum_{pn} \frac{\langle p\|\mathcal{O}_J\|n\rangle}{\sqrt{2J+1}}[c_p^+\tilde{c}_n]_{JM}, \qquad \text{(A6)}$$

we obtain

$$M_K = \sum_{J,\pi,k_i,k_f} \sum_{pnp'n'} (-)^J \frac{R}{g_A^2}$$

$$\times \int_0^\infty \frac{\mathcal{P}_{pnp'n',J}^K(q)}{|q|(|q| + (\Omega_{J^\pi}^{k_i} + \Omega_{J^\pi}^{k_f})/2)} h_K(q^2)q^2 dq$$

$$\times \langle 0_f^+\|[c_{p'}^+\widetilde{\tilde{c}_{n'}}]_J\|J^\pi k_f\rangle\langle J^\pi k_f|J^\pi k_i\rangle$$

$$\times \langle J^\pi k_i\|[c_p^+\tilde{c}_n]_J\|0_i^+\rangle. \qquad \text{(A7)}$$

Here $K = VV, MM, AA, PP, AP$, and

$$h_{VV}(\vec{q}^2) = -g_V^2(\vec{q}^2), \qquad h_{MM}(\vec{q}^2) = \frac{g_M^2(\vec{q}^2)\vec{q}^2}{4m_p^2},$$

$$h_{AA}(\vec{q}^2) = g_A^2(\vec{q}^2), \qquad h_{PP}(\vec{q}^2) = \frac{g_P^2(\vec{q}^2)\vec{q}^4}{4m_p^2}, \quad \text{(A8)}$$

$$h_{AP}(\vec{q}^2) = -2\frac{g_A(\vec{q}^2)g_P(\vec{q}^2)\vec{q}^2}{2m_p}.$$

The reduced matrix elements of the one-body operators $c_p^+\tilde{c}_n$ (the tilde denotes a time-reversed state) in Eq. (A8) depend on the BCS coefficients u_i, v_j and on the QRPA vectors X, Y [22]. The nuclear structure information resides in these quantities.

The $\mathcal{P}_{pnp'n',J}^K(q)$ in Eq. (A8) are products of the reduced one-body matrix elements of operators $\mathcal{O}^{(n)}(q)$:

$$\mathcal{P}_{pnp'n',J}^{VV}(q) = \langle p\|\mathcal{O}_J^{(1)}(q)\|n\rangle\langle p'\|\mathcal{O}_J^{(1)}(q)\|n'\rangle,$$

$$\mathcal{P}_{pnp'n',J}^{AA}(q) = \sum_{L=J,J\pm1} (-)^{J+L+1}$$

$$\times\langle p\|\mathcal{O}_{LJ}^{(2)}(q)\|n\rangle\langle p'\|\mathcal{O}_{LJ}^{(2)}(q)\|n'\rangle,$$

$$\mathcal{P}_{pnp'n',J}^{PP}(q) = \langle p\|\mathcal{O}_J^{(3)}(q)\|n\rangle\langle p'\|\mathcal{O}_J^{(3)}(q)\|n'\rangle,$$

$$\mathcal{P}_{pnp'n',J}^{AP}(q) = \mathcal{P}_{pnp'n',J}^{PP}(q),$$

$$\mathcal{P}_{pnp'n',J}^{MM}(q) = \mathcal{P}_{pnp'n',J}^{AA}(q) - \mathcal{P}_{pnp'n',J}^{PP}(q). \qquad \text{(A9)}$$

Here

$$\mathcal{O}_{JM}^{(1)}(q) = 2\sqrt{2}j_J(qr)Y_{JM}(\Omega_r),$$

$$\mathcal{O}_{LJM}^{(2)}(q) = 2\sqrt{2}j_L(qr)\{Y_L(\Omega_r)\otimes\sigma_1\}_{JM},$$

$$\mathcal{O}_{LJM}^{(3)}(q) = 2\sqrt{2}\sqrt{\frac{2J-1}{2J+1}}j_{J-1}(qr)C_{J-1010}^{J0}$$

$$\times\{Y_{J-1}(\Omega_r)\otimes\sigma_1\}_{JM}$$

$$-2\sqrt{2}\sqrt{\frac{2J+3}{2J+1}}j_{J+1}(qr)C_{J+1010}^{J0}$$

$$\times\{Y_{J+1}(\Omega_r)\otimes\sigma_1\}_{JM}. \qquad \text{(A10)}$$

The final step, leading to Eq. (4) in the text, is to rewrite the product of two one-body matrix elements as an appropriately recoupled (with pairs of protons and neutrons coupled to angular momentum $\mathcal{J}$) unsymmetrized two-body matrix element. Without the complications of angular momentum, this step simply reads

$$\langle p|O(1)|n\rangle\langle p'|O(2)|n'\rangle = \langle p, p'|O'(1,2)|n, n'\rangle. \quad \text{(A11)}$$

We then transform to relative and center-of-mass coordinates $\vec{r}_{12} = \vec{r}_1 - \vec{r}_2$ and $\vec{R}_{12} = (\vec{r}_1 + \vec{r}_2)/2$. Since the exchange potential depends only on $r_{12} = |\vec{r}_{12}|$ we end up with Eq. (4). The Fermi (F), Gamow-Teller (GT), and tensor (T) operators in that equation are

$$O_F(r_{12}, E_{J^\pi}^k) = \tau^+(1)\tau^+(2)H_F(r_{12}, E_{J^\pi}^k),$$

$$O_{GT}(r_{12}, E_{J^\pi}^k) = \tau^+(1)\tau^+(2)H_{GT}(r_{12}, E_{J^\pi}^k)\sigma_{12}, \quad \text{(A12)}$$

$$O_T(r_{12}, E_{J^\pi}^k) = \tau^+(1)\tau^+(2)H_T(r_{12}, E_{J^\pi}^k)S_{12}.$$

Here

$$\sigma_{12} = \vec{\sigma}_1 \cdot \vec{\sigma}_2,$$

$$S_{12} = 3(\vec{\sigma}_1 \cdot \hat{r}_{12})(\vec{\sigma}_2 \cdot \hat{r}_{12}). \qquad \text{(A13)}$$

The functions $h_K(q^2)$ that determine the H_K's through the integrals over q in Eq. (5) are

$$h_F(\vec{q}^2) = -g_A^2 h_{VV}(\vec{q}^2),$$

$$h_{GT}(\vec{q}^2) = \frac{1}{3}\left(2h_{MM}(\vec{q}^2) + h_{PP}(\vec{q}^2) + h_{AP}(\vec{q}^2)\right) + h_{AA}(\vec{q}^2),$$

$$h_T(\vec{q}^2) = \frac{1}{3}\left(h_{MM}(\vec{q}^2) - h_{PP}(\vec{q}^2) - h_{AP}(\vec{q}^2)\right),$$

$$\text{(A14)}$$

and the full matrix element is

$$M^{0\nu} = -\frac{M_F}{g_A^2} + M_{GT} + M_T. \qquad \text{(A15)}$$

Short-range repulsion can then be included as explained in Sec. IV.

APPENDIX B

Here we show how to calculate shell-model particle-hole decompositions so they can be compared with those calculated in the QRPA. To avoid too many complications, we will use the closure approximation. (In the text we have shown that, within the QRPA at least, using the closure approximation for the $0\nu\beta\beta$-decay results in an error of $\leqslant 10\%$.) The matrix element M (the subscript K is implied) can be written as in Eq. (4), with the overlap between intermediate-nucleus eigenstates a Kronecker delta if the those states are determined uniquely (as in the shell model). The matrix element M can be decomposed:

$$M = \sum_\alpha M^\alpha, \qquad \text{(B1)}$$

where α stands for the set of indices p, p', n, n' and

$$M^\alpha = \sum_{\mathcal{J}J} s_{\mathcal{J}J}^\alpha O_J^\alpha. \qquad \text{(B2)}$$

The parity index π is implicitly included along with J and $\mathcal{J}$. The O_J^α are given by

$$O_J^\alpha = \sum_{k_i,k_f} \langle 0_f^+ || [c_{p'}^+ \widetilde{\tilde{c}_{n'}}]_J || J^\pi k_f \rangle \langle J^\pi k_f | J^\pi k_i \rangle$$

$$\times \langle J^\pi k_i || [c_p^+ \tilde{c}_n]_J || 0_i^+ \rangle, \qquad (B3)$$

and the $s_{\mathcal{J}J}^\alpha$ are everything else in Eq. (4):

$$s_{\mathcal{J}J}^\alpha = (-1)^{j_n+j_{p'}+J+\mathcal{J}} \hat{\mathcal{J}} \begin{Bmatrix} j_p & j_n & J \\ j_{n'} & j_{p'} & \mathcal{J} \end{Bmatrix} Z_{\mathcal{J}}^\alpha, \qquad (B4)$$

with $\hat{\mathcal{J}} \equiv \sqrt{2\mathcal{J}+1}$ and

$$Z_J^\alpha \equiv \langle p(1), p'(2); \mathcal{J} \| \bar{f}(r_{12}) O_K \bar{f}(r_{12}) \| n(1), n'(2); \mathcal{J} \rangle. \qquad (B5)$$

(The $\bar{f}(r_{12})$ can be omitted if short-range correlations are included some other way.)

Now we can write M^α in two different ways:

$$M^\alpha = \sum_{\mathcal{J}} M_{\mathcal{J}}^{pp,\alpha} = \sum_J M_J^{ph,\alpha} \qquad (B6)$$

with

$$M_{\mathcal{J}}^{pp,\alpha} = \sum_J s_{\mathcal{J}J}^\alpha O_J^\alpha, \qquad (B7)$$

and

$$M_J^{ph,\alpha} = \sum_{\mathcal{J}} s_{\mathcal{J}J}^\alpha O_J^\alpha, \qquad (B8)$$

The $M_{\mathcal{J}}^{pp,\alpha}$ are the pp-hh amplitudes and the $M_J^{ph,\alpha}$ are the *ph* multipole-multipole amplitudes that we want to calculate in the shell model. All the nuclear structure information is in the O_J^α.

From Eq. (B7) we have

$$O_J^\alpha = \sum_{\mathcal{J}} s_{J\mathcal{J}}^{-1,\alpha} M_{\mathcal{J}}^{pp,\alpha}, \qquad (B9)$$

and

$$M_J^{ph,\alpha} = \sum_{\mathcal{J}} s_{\mathcal{J}J}^\alpha O_J^\alpha \xrightarrow{\text{[from Eq. (B9)]}}$$

$$\times \sum_{\mathcal{J}} s_{\mathcal{J}J}^\alpha \sum_{\mathcal{J}'} s_{J\mathcal{J}'}^{-1,\alpha} M_{\mathcal{J}'}^{pp,\alpha}. \qquad (B10)$$

So, exchanging the primed and unprimed labels in the sum, we can write the $M_J^{ph,\alpha}$ in terms of the $M_{\mathcal{J}}^{pp,\alpha}$ as

$$M_J^{ph,\alpha} = \sum_{\mathcal{J},\mathcal{J}'} s_{\mathcal{J}'J}^\alpha s_{J\mathcal{J}}^{-1,\alpha} M_{\mathcal{J}}^{pp,\alpha}. \qquad (B11)$$

The final particle-hole multipole contribution that we want is then just

$$M_J^{ph} \equiv \sum_\alpha M_J^{ph,\alpha}. \qquad (B12)$$

From the relation

$$\hat{J}^2 \sum_X \hat{X}^2 \begin{Bmatrix} a & b & J \\ c & d & X \end{Bmatrix} \begin{Bmatrix} a & b & J' \\ c & d & X \end{Bmatrix} = \delta_{J,J'} \qquad (B13)$$

we have

$$s_{J\mathcal{J}}^{-1,\alpha} = (-1)^{j_n+j_{p'}+J+\mathcal{J}} \frac{\hat{J}^2\hat{\mathcal{J}}}{Z_{\mathcal{J}}^\alpha} \begin{Bmatrix} j_p & j_n & J \\ j_{n'} & j_{p'} & \mathcal{J} \end{Bmatrix}. \qquad (B14)$$

Finally, putting everything together, we get

$$M_J^{ph} \equiv \sum_{p,p',n,n',\mathcal{J}\mathcal{J}'} (-1)^{\mathcal{J}+\mathcal{J}'} \hat{\mathcal{J}}\hat{\mathcal{J}}'\hat{J}^2 \begin{Bmatrix} j_p & j_n & J \\ j_{n'} & j_{p'} & \mathcal{J}' \end{Bmatrix}$$

$$\times \begin{Bmatrix} j_p & j_n & J \\ j_{n'} & j_{p'} & \mathcal{J} \end{Bmatrix} \frac{Z_{\mathcal{J}'}^\alpha}{Z_{\mathcal{J}}^\alpha} M_{\mathcal{J}}^{pp,\alpha}. \qquad (B15)$$

In a shell model calculation, one can write the double beta-decay matrix element solely in terms of antisymmetrized matrix elements of the corresponding operator. But to obtain the particle-hole decomposition above, the natural definition since the operator really represents a product of two one-body currents, one must start from a representation of the operator in terms of *unsymmetrized* matrix elements $Z_{\mathcal{J}}^\alpha$

$$\hat{O}_K = -\frac{1}{2} \sum_{p,n,p',n',\mathcal{J}} Z_{\mathcal{J}}^\alpha [[a_{j_p}^\dagger a_{j_{p'}}^\dagger]^{\mathcal{J}} [\tilde{a}_{j_n} \tilde{a}_{j_{n'}}]^{\mathcal{J}}]^0, \quad (B16)$$

and calculate the $M_{\mathcal{J}}^{pp,\alpha}$, for all $\alpha \equiv p, p', n, n'$, not just $p \geqslant p', n \geqslant n'$.

[1] R. D. McKeown and P. Vogel, Phys. Rep. **394**, 315 (2004).

[2] S. M. Bilenky, C. Giunti, J. A. Grifols, and E. Massó, Phys. Rep. **379**, 69 (2003).

[3] P. Langacker, Int. J. Mod. Phys. A **20**, 5254 (2005); hep-ph/0411116.

[4] A. Strumia and F. Vissani, hep-ph/0606054.

[5] G. L. Fogli, E. Lisi, A. Marrone, and A. Palazzo, Prog. Part. Nucl. Phys. **57**, 742 (2006).

[6] A. Faessler and F. Šimkovic, J. Phys. G **24**, 2139 (1998).

[7] J. D. Vergados, Phys. Rep. **361**, 1 (2002).

[8] S. R. Elliott and P. Vogel, Annu. Rev. Nucl. B Part. Sci. **52**,115 (2002); S. R. Elliott, Nucl. Phys. B Proc. Suppl. **138**, 275 (2005).

[9] S. R. Elliott and J. Engel, J. Phys. G **30**, R183 (2004).

[10] Frank T. Avignone III, Steven R. Elliott, and Jonathan Engel, Rev. Mod. Phys. (to be published); arXiv:0708.1033v1 [nucl-ex].

[11] S. J. Freedman and B. Kayser, physics/0411216 (see also http://www.aps.org/neutrino/ for more details).

[12] C. Aalseth *et al.*, hep-ph/0412300.

[13] V. A. Rodin, A. Faessler, F. Šimkovic, and P. Vogel, Phys. Rev. C **68**, 044302 (2003).

[14] V. A. Rodin, A. Faessler, F. Šimkovic, and P. Vogel, Nucl. Phys. **A766**, 107 (2006) erratum; **A793**, 213 (2007); arXiv:0706.4304.

[15] E. Caurier, F. Nowacki, and A. Poves, arXiv:0709.0277 [nucl-th].

[16] E. Caurier, J. Menéndez, F. Nowacki, and A. Poves, Phys. Rev. Lett. **100**, 052503 (2008).

[17] J. Engel and P. Vogel, Phys. Rev. C **69**, 034304 (2004).

[18] J. Menéndez, A. Poves, E. Caurier, and F. Nowacki, preprint arXiv:0801.3760.

[19] M. Kortelainen, O. Civitarese, J. Suhonen, and J. Toivanen, Phys. Lett. **B647**, 128 (2007).

[20] M. Kortelainen and J. Suhonen, Phys. Rev. C **75**, 051303(R) (2007).

[21] M. Kortelainen and J. Suhonen, Phys. Rev. C **76**, 024315 (2007).

[22] F. Šimkovic, G. Pantis, J. D. Vergados, and A. Faessler, Phys. Rev. C **60**, 055502 (1999).

[23] A. Poves (private communication).

[24] H. Feldmeier, T. Neff, R. Roth, and J. Schnack, Nucl. Phys. **A632**, 61 (1998).

[25] A. Fabrocini, F. A. de Saavedra, and G. Co', Phys. Rev. C **61**, 044302 (2000); G. Co' (private communication).

[26] G. A. Miller and J. E. Spencer, Ann. Phys. (NY) **100**, 562 (1976).

[27] S. M. Bilenky and S. Petcov, Rev. Mod. Phys. **59**, 671 (1987).

[28] T. Ericson and W. Weise, *Pions and Nuclei* (Clarendon, Oxford, 1988), pp. 423.